Polyketides

Deutsche Ausgabe: DOI: 10.1002/ange.201507418
Internationale Ausgabe: DOI: 10.1002/anie.201507418

Stereochemical Studies of the Karlotoxin Class Using NMR Spectroscopy and DP4 Chemical-Shift Analysis: Insights into their Mechanism of Action

*Amanda L. Waters, Joonseok Oh, Allen R. Place, and Mark T. Hamann**

Abstract: *After publication of karlotoxin 2 (KmTx2; **1**), the harmful algal bloom dinoflagellate Karlodinium sp. was collected and scrutinized to identify additional biologically active complex polyketides. The structure of **1** was validated and revised at C49 using computational NMR tools including J-based configurational analysis and chemical-shift calculations. The characterization of two new compounds [KmTx8 (**2**) and KmTx9 (**3**)] was achieved through overlaid 2D HSQC NMR techniques, while the relative configurations were determined by comparison to **1** and computational chemical-shift calculations. The detailed evaluation of **2** using the NCI-60 cell lines, NMR binding studies, and an assessment of the literature supports a mode of action (MoA) for targeting cancer-cell membranes, especially of cytostatic tumors. This MoA is uniquely different from that of current agents employed in the control of cancers for which **2** shows sensitivity.*

The karlotoxins are a suite of compounds which have hemolytic, cytotoxic, and ichthyotoxic activity.[1] At least eight distinct strains of *Karlodinium* sp. have been isolated from around the world, and each produce their own suite of compounds.[2] There has been a tremendous amount of research on the configurational assignment and mode of action (MoA) of the KmTx's, and it is driven by the structural similarity of **1**[3] to amphidinol 3 (Am3; **4**), which was isolated from *Amphidinium* sp (Figure 1).[4] While they share remarkable structural similarity and are probably derived from the same biosynthetic machinery, the pyran sections (C28–C49 in **1** and C30–C51 in **4**) of the molecules are published with the enantiomeric configurations.[4] The absolute configuration of **4** was determined based on *J*-based configurational analysis (*J*BCA), NOE interactions, and a modified Mosher's method,[4] while that of **1** was assigned using *J*BCA, NOE interactions, degradation with Grubbs II catalyst, and periodate-mediated diol degradation.[3a] Am3 (**4**) has already undergone two relative configuration revisions, C2 in 2008 and C51 in 2013.[5] With the advancements of computational methodologies, the computationally assisted *J*BCA and chemical-shift (CS) calculations of **1** were undertaken to further assess the assigned configuration of the KmTx class.

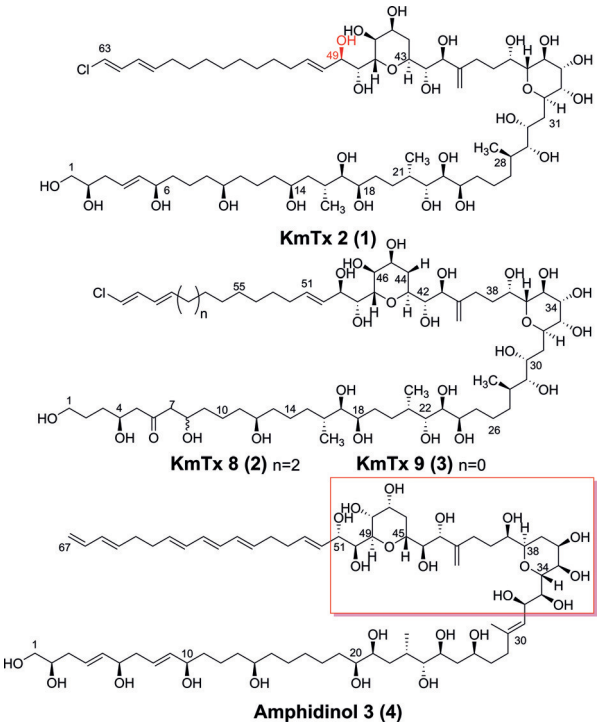

Figure 1. Complex polyketide natural products derived from *Karlodinium* and *Amphidinium* sp.: KmTx2 (**1**),[3a] KmTx8 (**2**), KmTx9 (**3**), and Am3 (**4**).[4] The revised stereochemistry at C49 for **1** is shown. The red box indicates the deviation in the stereochemistry of the pyran systems between **1** and **4**.

The revision for the relative configuration of the C50–C51 bond in **4**[5a] warranted verifying the assignment for the corresponding bond in **1** (C48–C49). The revision of **4** at C51 was confirmed using the gauge-including atomic orbital (GIAO) NMR CS calculation. This served both as validation for the method on a molecule of this size and further confirmation of the revision of **4** (Figure 2). The $^{2}J_{(C51,\ H50)}$ value of −2.5 Hz is considered an "intermediate" value, which may have led to the misassignment of C51.[6]

[*] Dr. A. L. Waters,[+] Dr. J. Oh,[+] Prof. M. T. Hamann
Department of Pharmacognosy, Pharmacology, School of Pharmacy, and Department of Chemistry and Biochemistry, University of Mississippi, University, MS 38677 (USA)
E-mail: mthamann@olemiss.edu
Prof. M. T. Hamann
Department of Drug Discovery and Biomedical Sciences
Medical University of South Carolina
Charleston, SC 29425 (USA)
E-mail: hamannm@musc.edu
Prof. A. R. Place
Institute of Marine and Environmental Technology, University of Maryland Center for Environmental Sciences
Suite 236 Columbus Center, Baltimore, MD 21202 (USA)
[+] These authors contributed equally to this work.

Supporting information for this article is available on the WWW under http://dx.doi.org/10.1002/anie.201507418.

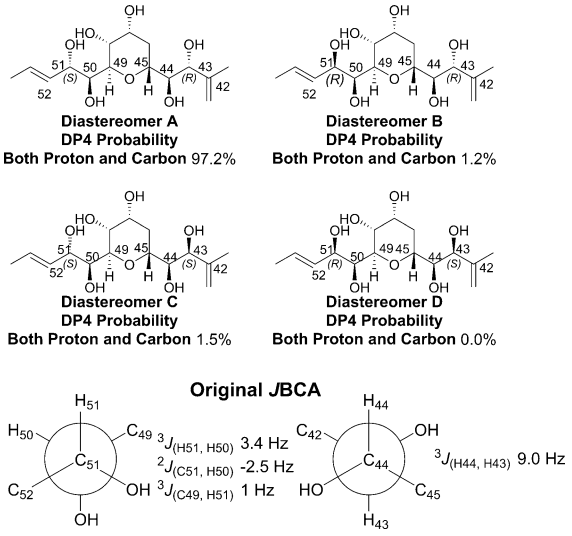

Figure 2. Confirmation of the structural revision of **4** using DP4 calculations. Shown are the diastereomers A–D for the relative configuration revision at C51 and the DP4 probability supporting the structural revisions made by Ebine et al.[5a] Also shown are the original *J*BCA for **4**: $^{2}J_{(C51,H50)}$ value of −2.5 Hz is considered an intermediate value, thus resulting in the misassignment of C51. The large value for $^{3}J_{(H44,H43)}$ leads to an unambiguous assignment.

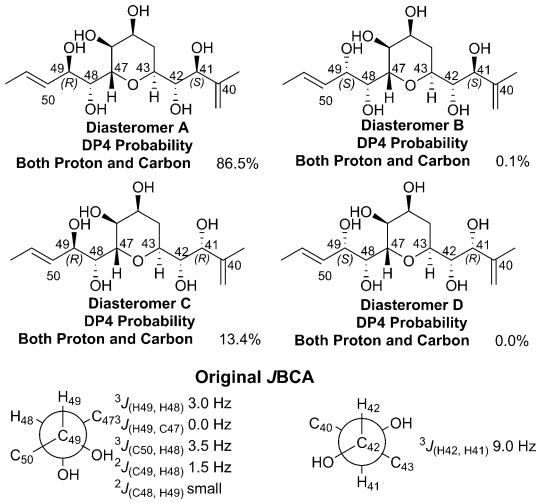

Figure 3. Confirmation of the structural revision of karlotoxin using DP4 calculations. Shown are the four diastereomers used to investigate the revision of the relative configuration at C49 and C41, based on the amphidinol 3 revision. Also shown is the original *J*BCA for **1**: $^{3}J_{(C50,H48)}$ value of 3.5 Hz is considered an intermediate value, thus resulting in the misassignment of C49. The large value for $^{3}J_{(H42,H41)}$ leads to an unambiguous assignment of configuration.

The same method was explored to identify if a similar revision was necessary for **1**. The "large" values (7–10 Hz for this diol system) for $^{3}J_{H,H}$ are indicative of a structure with no significant conformational changes occurring, thus giving a reliable *J*BCA.[6] Four possible diastereomers of C40–C51 were designed. The bonds between C42–C43, C47–C48, and the pyran were constrained based on NOE interactions and *J*BCA as previously described. Even though $^{2}J_{(C47,H48)}$ fell into the intermediate range,[3a] the C47–C48 bond was also constrained given the large $^{3}J_{(H47,H48)}$ value,[3a] thus indicating no major conformational conversion occurred in this bond.[6] The DP4 probability analysis was conducted with experimental and predicted CS values of the four diastereomers and the results indicated that 41*S*,49*R* was the most relevant with a probability of 86.5 % (Figure 3). This outcome implies that the original relative assignment of C48–C49, based on *J*BCA, is incorrect and the revision for **4** also holds true for **1**. As in **4**, the $^{3}J_{(C50,H48)}$ value of 3.5 Hz for **1** is considered an intermediate value, which may have resulted in the misassignment of C49. These calculations suggest that *J*BCA assignments should be employed with care, especially when dealing with intermediate and "small" coupling values and, when appropriate, confirmed using the CS calculation method, unless a vicinal coupling constant of two protons in an associated bond is large.[6]

The next approach to verifying the absolute configuration of **1** was to use computation methods to validate the *J*BCA. The *J*BCA of C28–C29 resulted in an intermediate vicinal homocoupling constant value.[3a] As such, computation analysis of the three staggered conformers at that position gave us calculated values to compare with the measured values (Figure 4). The C28-position was determined, based on degradation analysis, to be the *R* configuration,[3a] so for the

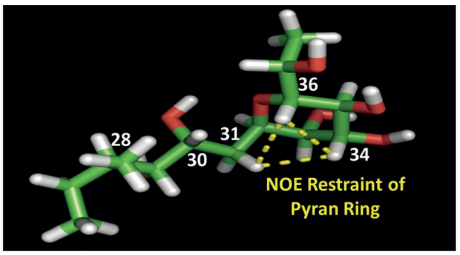

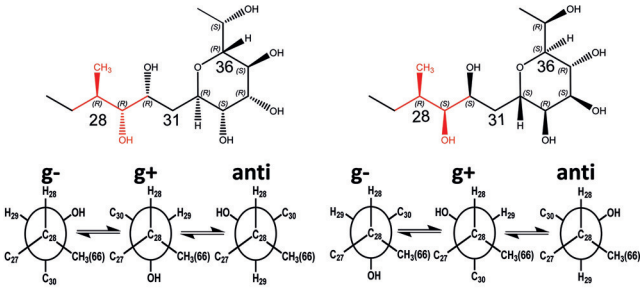

Conformation between H29 and H28	gauche⁻	gauche⁺	anti	Exp.	gauche⁻	gauche⁺	anti
$^{3}J_{(H-29,H-28)}$	4.30	1.77	9.34	7.3	1.79	4.23	9.36
$^{3}J_{(C-66,H-29)}$	5.95	4.10	1.84	2.0	6.12	1.98	2.66
$^{2}J_{(C-29,H-28)}$	-5.34	0.08	-5.28	-4.6	0.45	-5.48	-5.18
Total Absolute Deviation	7.69	12.31	2.89	0	14.68	3.97	3.31

Figure 4. Computational analysis of the coupling constants for the C27–C30 assignment of **1** and inversion of stereochemistry starting at C29 by using three different conformations (*gauche*$^{+}$, *gauche*$^{-}$, *anti*). The values are compared with the experimental values by total absolute deviation calculations. Dashed yellow line in the three-dimensional representation indicates NOE correlations employed to restrain the tetrahydropyran ring.

analysis this position remained fixed. For comparison, the three conformers of the opposite configuration, starting at C29, were also analyzed. The relative configuration of C29–C32 on both models was fixed based on the *J*BCA and the structures were minimized. The NOE data from **1** were also analyzed and integrated to establish distance restraints for the tetrahydropyran rings. After restraints were applied, a conformation search was conducted using Schrödinger MacroModel. Using an 80% or higher Boltzmann distribution cutoff, the conformers were optimized and the coupling constant values were calculated using Gaussian 09. The total absolute deviation (TAD) was used for the comparison of the absolute value of the difference between the calculated and the experimental values. The CS values for **1** were also analyzed using both mean absolute error calculations and DP4 probability statistics.[7] The computation work supports the published relative configuration of C28–C29 of **1** in the *anti* conformation, which has the lowest TAD value at 2.89.

Given that the GIAO NMR CS calculations have been validated to correctly assign the relative configuration of certain stereogenic centers in **1**, the extension of this methodology was attempted to verify ambiguities of the *J*BCA in the original assignment. It is important to note that earlier attempts at analyzing these data using only fragments of the structure provided unreliable results depending on the length of the fragment being analyzed. When analyzing the larger, flexible fragments, the entire structure of **1** was assessed using the DP4 applet.[7a] The results showed that for the relative configuration assignments of the published structure of **1**, for C36–C37 and C28–C29, the highly flexible bonds deduced from the medium values of $^{3}J_{(H36,H37)}$ and $^{3}J_{(H28,H29)}$, respectively, were correct (Figure 5).

By capitalizing on the extensive NMR data collected for **1**, a two-dimensional heteronuclear single quantum coherence (HSQC) NMR overlay experiment was utilized to determine the planar structure of **2**, which isolated from an Australian *K. veneficum* strain.[8] The NMR data alluded to the loss of an olefinic moiety between C4 and C5 with the addition of the oxidation of the hydroxy group at C6 to a carbonyl functionality. The appearance of a carbon center resonating at $\delta =$ 211.94 ppm indicated the presence of a ketocarbonyl moiety, and the alteration of the CS values for C5 and C7 to $\delta =$ 51.94 ppm and $\delta = 52.04$ ppm, respectively, by HMBC, assigned its position. The loss of the hydroxy group on C2 was also observed. The remaining differences in oxidation from C1–C18 were confirmed by HMBC and COSY correlations which trace the correlations from C1 through C5 and then again from C7 through C16. KmTx9 (**3**) was isolated from a closely related species *K. conicum*, which came from the most southern and coldest location of all of the species isolated to date.[2] The HSQC data for **2** and **3** overlaid well with the exception of increased signal intensity for **2** in the C53–C56 region. This data coupled with the loss of 28 amu between the masses of **2** and **3** was a strong indication of a shortening of the aliphatic chain by two methylene units. The relative configuration of **2** and **3** was assigned by comparison to **1**. For the portions of **2** and **3** that were too different for direct comparison by NMR spectroscopy, CS calculations were completed to confirm the relative configuration of the new stereogenic centers and link them to the known absolute configuration of C21 as established for **1** by degradation chemistry.

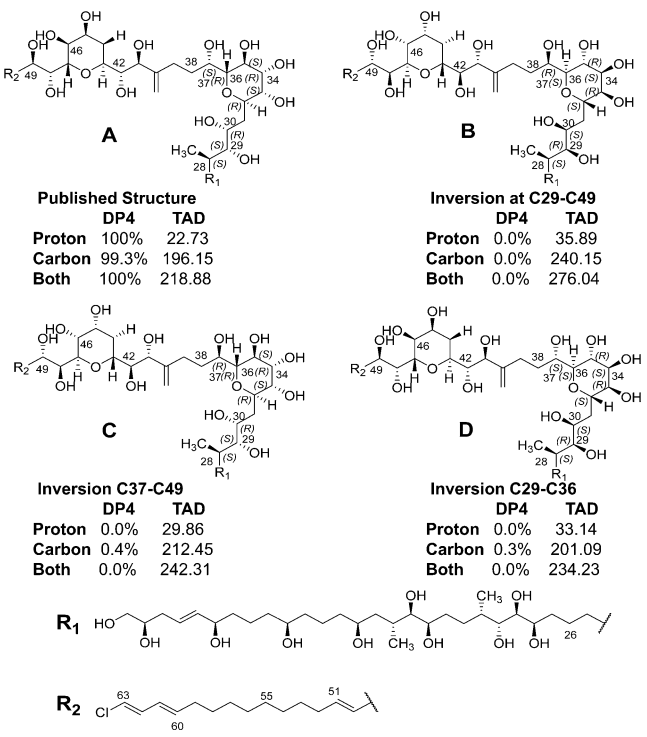

Figure 5. Four possible diastereomers for GIAO NMR shift analysis of **1**. A) The published structure of **1**[3a] with C49 modification. B) Inversion of stereochemistry at C29–C49. C) Inversion of stereochemistry C37–C49. D) Inversion of stereochemistry at C29–C36.

Next, the GIAO NMR CS calculations were used to establish the relative configuration of stereogenic centers in the polyol section of **2**, a section which is identical to that in **3**. For validation of the method on a polyol chain, four different diastereomers of **1** were employed with varying configurations at C6 and C10, and a GIAO NMR CS analysis was performed. Based on these results, the DP4 method provided data which were consistent with the relative configuration of **1**, the configuration that was established by Mosher's ester analysis. The 6*R*,10*R* diastereomer showed the lowest TAD and a 100% probability of being the correct assignment (Figure S1 in the Supporting Information). By using the same technique, the relative configuration of the polyol chain of **2** was analyzed. Every carbon atom that did not have a direct overlap with the HSQC of **1** was analyzed. This approach not only allowed the determination of the relative configuration of the polyol chain, but also relayed it back to the absolute configuration which was determined for C21 in **1**. This method gave a conclusive answer for all but one of the undetermined stereocenters (4*S*,12*R* with C8 remaining ambiguous) (Figure S2 in the Supporting Information). The proton TAD and DP4 calculations supported one diastereomer and the carbon TAD and DP4 supported another diastereomer with only one stereocenter being opposite. Interestingly, when both carbon and proton data were taken

into account for the DP4 analysis a different diastereomer with no discernible pattern was supported (Figure S2 in the Supporting Information). It is clear that this result occurs because such a diastereomer strikes a balance between the lowest TAD for proton and carbon, and is statistically not unexpected.

Studies have elucidated the ecological role of **1** as being that of a prey-capture mechanism. A pore is formed in the cell membrane with certain sterol interactions, thus disturbing the osmotic balance of the cell through membrane depolarization and ultimately leading to cell death through osmotic lysis.[9] This MoA is dependent in part on the sterol composition of the cell.[2,9b] Cells containing 4α-methyl sterols are resistant to **1**, whereas cells containing 4-desmethyl sterols (like cholesterol) are sensitive to **1**.[10] Studies also show that this lysis event is preceded by the permeabilization of the plasma membrane to various cations, including Ca^{2+}, Na^{+}, and K^{+}. Presumably, these same pores also allow the disruption of the osmotic balance in the cell leading to cell death.[11] Studies for **4** have shown a similar affinity for phospholipid membranes which contain sterols and transmembrane proteins. Sterols and protein-containing membranes play an important role in the mechanism of action which has been shown to be pore or lesion formation.[12] Still under investigation is whether this pore follows the hypothesized barrel-stave model as predicted for amphotericin B, or a toroidal pore model as predicted for **4**.[13] The configuration of the sterol 3-OH group has also been shown to be important for activity in this class of molecules. For **4**, pore formation was only seen when 3β-OH sterols were present in the membrane and not in the presence of 3α-OH sterols such as epicholesterol.[14]

HSQC overlay studies were conducted to provide further insight into the sterol-binding interactions of the karlotoxins. By using a series of increasing ratios of cholesterol added to **2**, HSQC NMR experiments were conducted. Figure 7b summarizes the atoms that were perturbed by the addition of cholesterol. There were definitive shifts for certain carbon atoms, mainly around the tetrahydropyran ring systems, while other carbon atoms (e.g., C1) on the exterior of the structure were untouched by the addition of cholesterol. Based on the cholesterol interactions, the molecule appears to prefer a hairpin formation, which has not been seen when the molecule is freely rotating without other molecular interactions. ROESY experiments were also performed with these samples, however, the solubility limitations restricted the solvent choices for **2** with cholesterol and no meaningful NOE interactions were observed.

KmTx8 (**2**) exhibited hemolysis using rainbow trout erythrocytes with $HD_{50} = (0.049 \pm 0.004)$ μM, thus making it the most hemolytic compound at over 26 times the potency of KmTx2 [**1**; $HD_{50} = (1.3 \pm 0.3)$ μM]. KmTx9 (**3**) was the least active of any compound assayed to date [$HD_{50} = (3.0 \pm 0.3)$ μM]. This data indicated that the length of the lipophilic chain is important to the overall MoA of the molecule, perhaps through perturbations in lipid bilayer interactions. When **1** was injected into 10 female Balb/c mice IP, no lethality was observed, even at a high dose of 500 $\mu g\,kg^{-1}$. The only physical effects noted were reversible anorexia and a single case of necrotizing pancreatitis.[15]

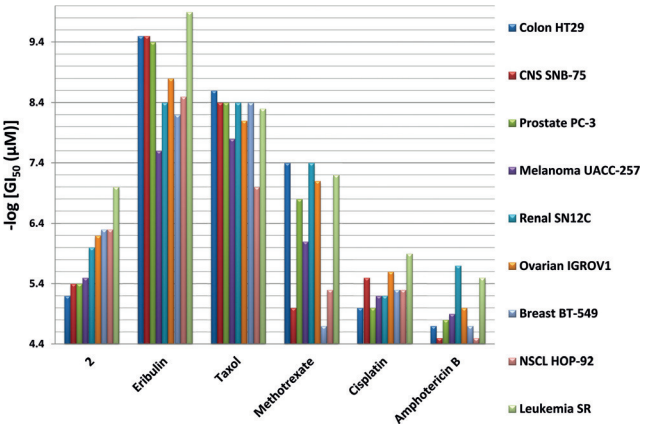

Figure 6. Comparison of select NCI 60 cell panel GI_{50} for **2** versus controls.

In the NCI-60 cell panel, **2** was most sensitive for leukemia cell lines SR ($GI_{50} = 0.100$ μM) and CCRF-CEM ($GI_{50} = 0.686$ μM), non-small cell lung cancer lines HOP-62 ($GI_{50} = 0.986$ μM), NCI-H23 ($GI_{50} = 0.903$ μM) and HOP-92 ($GI_{50} = 0.501$ μM), ovarian cancer cell line IGROV1 ($GI_{50} = 0.631$ μM), renal cancer cell line SN12C ($GI_{50} = 1.000$ μM), and breast cancer cell line BT-549 ($GI_{50} = 0.501$ μM). Figure 6 illustrates how **2** compares to other FDA-approved cancer drugs [eribulin (NSC 707389), taxol (NSC 125973), methotrexate (NSC 740), and cisplatin (NSC 119875]), as well as amphotericin B (AmB; NSC 527017) which has a similar structure and a mechanism known to involve sterol binding.[16] KmTx8 (**2**) was also screened in HeLa cells ($GI_{50} = 369$ nM, $TGI = 609$ nM, $LC_{50} = 1064$ nM). In addition, a cell cycle analysis was performed and showed that there were no changes in cell cycle distribution after treatment with **2**. This data indicates that the MoA is independent of cell division, thus opening the door to treating both aggressively replicating and cytostatic cancer types, and possibly reducing off-target toxicity issues commonly associated with various parts of the cell cycle.

Comparison of **2** against all publically available NCI-60 data using the CellMiner Database Version 1.4,[17] the Compare[18] algorithm, and Pearson correlation coefficients were performed. The Pearson correlation for **2** with AmB is 0.254. Any value under 0.7 is considered statistically insignificant. Therefore, **2** and AmB do not share a similar MoA based on their NCI-60 data. However, it is possible that the activity of **2** is due to interactions with multiple targets in addition to sterol interactions. This behavior would explain the low correlation to AmB. Further studies are needed to address the similarity of the MoA. The closest correlation to **2** was a synthetic product, which is not in clinical trials, where the MoA has not been defined [citratohydratogallium(III), 0.766]. By using this same resource, the mining of gene correlations which are either up- or down-regulated for **2** was also explored. By using the search tool for the retrieval of interacting genes/proteins (STRING) 9.0 database, further downstream and upstream targets in the MoA pathway were identified for the top 10 gene correlations.[19] All but four correlations share a common pathway. This pathway appears to be heavily influenced by

extracellular receptors (IL2RA and IL2B) imbedded in the cell membrane.

Given that the already established MoA is the permeabilization of the plasma membrane, our hypothesis is that the sterol binding interactions of **2** are affecting the stability of the cell membrane, thereby having an impact on membrane integrity and possibly cellular signaling, which depends on extracellular receptors to function properly. The pore formed by **2** appears similar to an aquaporin or water channel based on activity. This is further supported by the 0.644 correlation with Aquaporin 9. While the value is only marginally significant, it implies that a pore-forming mechanism affecting osmotic balance might be responsible for the activity. ABCA1, a protein responsible for transfer of cellular cholesterol across the plasma membrane, has been shown to play a role in the buildup of cholesterol in cancer cells over normal cells leading to avoidance of the normal cell-death signaling cycle.[20] These data further support the mechanistic rationale for cholesterol-targeting as a potential cancer treatment strategy.

Given the aqueous nature of the cellular environment, it is hypothesized that KmTx forms a pore with multiple molecules in a micelle-like interaction. This formation is also seen in previous studies on **4**.[13a] While it is understood that the limitations of solubility of KmTx's and sterols limits the ability of the NMR binding experiment to closely mimic the aqueous external membrane environment, the results from this study corroborate what has previously been seen for **4**. These interactions would aid the pore formation of KmTx in the sterol-containing cellular membrane. The proposed interaction of KmTx on a cell membrane is shown in Figure 7. The data supports that the sterol interactions are a vital part of the MoA, while it is hypothesized that the length of the lipophilic chain interacts with another portion of the membrane, possibly the phospholipids, to strengthen the interaction. The 3-OH of the sterol group is likely heavily involved in hydrogen bonding at the apex of the proposed hairpin structure, while van der Waals forces strengthen the binding of the polyene section of KmTx to the lipophilic tail of the sterol. Having a sufficient chain length is critical to activity as seen in the difference of hemolysis of **2** and **3**. It is likely that the shorter chain length of **3** does not allow multiple molecules to stabilize each other as well as the longer chain length does. The lack of stabilization results in fewer pores being able to form, thus leading to the decrease in activity. The degree of hydroxylation of the molecule is hypothesized to be equally important to provide stabilizing hydrogen bonds with the transmembrane proteins and other KmTx molecules.

This suite of molecules exhibits an interesting cytotoxic MoA through cholesterol and other membrane binding interactions. Based on computational data and comparison with the structural revisions made to **4**, a minor stereochemical revision was made to the KmTx scaffold at C49.[5a] Furthermore, this new data, using the DP4 calculations, supports the published relative configuration of **1** at C28 through C37. By mining the NCI-60 cytotoxic activity of **2**, it is clear that this class of molecules provides cell sensitivity for certain tumor cell groups. The specific interactions and structural details, which yield tumor-cell sensitivity for NSCLC and leukemia, remains to be determined. However, the data presented here reveals that preparing tumor-cell-selective, pore-forming agents is a possibility that must be explored in the development of new chemotherapeutic agents for the control of cancer.

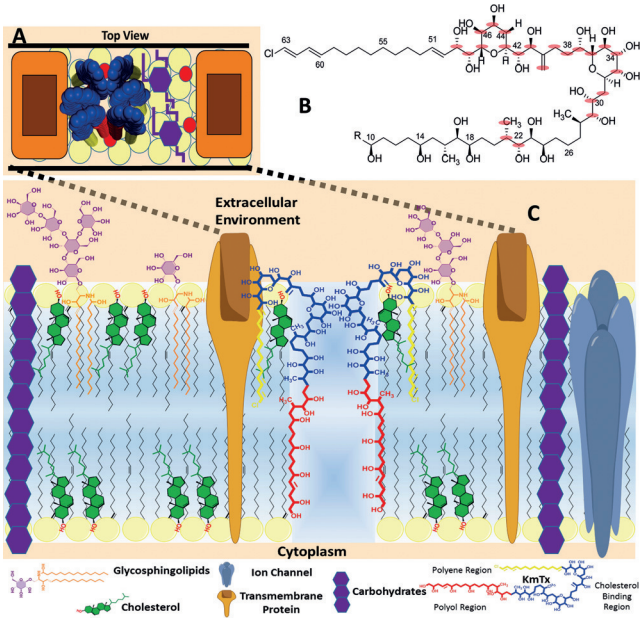

Figure 7. Hypothesis for MoA of KmTx. A) Proposed pore formation of multiple KmTx molecules in a top-down view of the cell membrane. B) Diagram of atoms affected by cholesterol interaction, based on HSQC perturbation experiments. C) Diagram of KmTx interactions forming pores inside the cell membrane.

Acknowledgments

We thank the NCI for their screening of **2**, Mooberry Lab at UTHSCSA for cell cycle analysis Mississippi Center for Supercomputing Research for supercomputer access, and Dr. M. Lodewyk and Dr. J. M. Goodman for advice and assistance with the computational work. This is contribution #5089 from UMCES, #15-164 for IMET, and #709 from the ECOHAB program. This research was supported by NIAID, CDC, NOAA, and MD DHMH and funded in part by grants from OHH NIH R01ES021949-01/NSFOCE1313888, NIH/NCCAM 1RO1AT007318, NSF GRFP No. 1144250, and NIH/NCRR C06 RR-14503-01.

Keywords: cancer · computational chemistry · membranes · natural products · polyketides

How to cite: *Angew. Chem. Int. Ed.* **2015**, *54*, 15705–15710
Angew. Chem. **2015**, *127*, 15931–15936

[1] a) J. R. Deeds, D. E. Terlizzi, J. E. Adolf, D. K. Stoecker, A. R. Place, *Harmful Algae* **2002**, *1*, 169–189; b) J. W. Kempton, A. J. Lewitus, J. R. Deeds, J. M. Law, A. R. Place, *Harmful Algae* **2002**, *1*, 233–241.

[2] B. D. Mooney, M. de Salas, G. M. Hallegraeff, A. R. Place, *J. Phycol.* **2009**, *45*, 164 – 175.
[3] a) J. Peng, A. R. Place, W. Yoshida, C. Anklin, M. T. Hamann, *J. Am. Chem. Soc.* **2010**, *132*, 3277 – 3279; b) R. M. Van Wagoner, J. R. Deeds, M. Satake, A. A. Ribeiro, A. R. Place, J. L. C. Wright, *Tetrahedron Lett.* **2008**, *49*, 6457 – 6461; c) J. Peng, R. Hill, A. Place, C. Anklin, M. T. Hamann, in Abstracts of Papers, 233rd ACS National Meeting, March 25 – 29, **2007**, pp. AGFD-030.
[4] M. Murata, S. Matsuoka, N. Matsumori, G. K. Paul, K. Tachibana, *J. Am. Chem. Soc.* **1999**, *121*, 870 – 871.
[5] a) M. Ebine, M. Kanemoto, Y. Manabe, Y. Konno, K. Sakai, N. Matsumori, M. Murata, T. Oishi, *Org. Lett.* **2013**, *15*, 2846 – 2849; b) T. Oishi, *Org. Lett.* **2008**, *10*, 5203 – 5206.
[6] N. Matsumori, D. Kaneno, M. Murata, H. Nakamura, K. Tachibana, *J. Org. Chem.* **1999**, *64*, 866 – 876.
[7] a) S. G. Smith, J. M. Goodman, *J. Am. Chem. Soc.* **2010**, *132*, 12946 – 12959; b) S. G. Brown, M. J. Jansma, T. R. Hoye, *J. Nat. Prod.* **2012**, *75*, 1326 – 1331.
[8] J. E. Adolf, T. R. Bachvaroff, J. R. Deeds, A. R. Place, *Harmful Algae* **2015**, *48*, 83 – 93.
[9] a) A. L. Waters, R. T. Hill, A. R. Place, M. T. Hamann, *Curr. Opin. Biotechnol.* **2010**, *21*, 780 – 786; b) J. Sheng, E. Malkiel, J. Katz, J. E. Adolf, A. R. Place, *Proc. Natl. Acad. Sci. USA* **2010**, *107*, 2082 – 2087.
[10] a) J. R. Deeds, A. R. Place, *Afr. J. Mar. Sci.* **2006**, *28*, 421 – 425; b) A. R. Place, X. M. Bai, S. J. Kim, M. R. Sengco, D. W. Coats, *J. Phycol.* **2009**, *45*, 375 – 385.
[11] J. R. Deeds, R. E. Hoesch, A. R. Place, J. P. Kao, *Aquat. Toxicol.* **2015**, *159*, 148 – 155.
[12] a) R. T. Swasono, R. Mouri, N. Morsy, N. Matsumori, T. Oishi, M. Murata, *Bioorg. Med. Chem. Lett.* **2010**, *20*, 2215 – 2218; b) N. Morsy, K. Konoki, T. Houdai, N. Matsumori, T. Oishi, M. Murata, S. Aimoto, *Biochim. Biophys. Acta Biomembr.* **2008**, *1778*, 1453 – 1459; c) N. Morsy, T. Houdai, S. Matsuoka, N. Matsumori, S. Adachi, T. Oishi, M. Murata, T. Iwashita, T. Fujita, *Bioorg. Med. Chem.* **2006**, *14*, 6548 – 6554.
[13] a) N. Matsumori, M. Murata, *Nat. Prod. Rep.* **2010**, *27*, 1480 – 1492; b) A. Neumann, M. Baginski, J. Czub, *J. Am. Chem. Soc.* **2010**, *132*, 18266 – 18272.
[14] R. A. Espiritu, N. Matsumori, M. Tsuda, M. Murata, *Biochemistry* **2014**, *53*, 3287 – 3293.
[15] A. R. Place, R. Munday, J. Munday, *Toxicon* **2014**, *90*, 184 – 190.
[16] M. Baginski, J. Czub, *Curr. Drug Metab.* **2009**, *10*, 459 – 469.
[17] W. C. Reinhold, M. Sunshine, H. Liu, S. Varma, K. W. Kohn, J. Morris, J. Doroshow, Y. Pommier, *Cancer Res.* **2012**, *72*, 3499 – 3511.
[18] B. N. Zhou, J. M. Hoch, R. K. Johnson, M. R. Mattern, W. K. Eng, J. Ma, S. M. Hecht, D. J. Newman, D. G. Kingston, *J. Nat. Prod.* **2000**, *63*, 1273 – 1276.
[19] D. Szklarczyk, A. Franceschini, M. Kuhn, M. Simonovic, A. Roth, P. Minguez, T. Doerks, M. Stark, J. Muller, P. Bork, L. J. Jensen, C. von Mering, *Nucleic Acids Res.* **2011**, *39*, D561 – D568.
[20] B. Smith, H. Land, *Cell Rep.* **2012**, *2*, 580 – 590.

Received: August 9, 2015
Revised: September 22, 2015
Published online: November 16, 2015

